Aerosol and Air Quality Research, 15: 994–1007, 2015

ISSN: 1680-8584 print / 2071-1409 online
doi: 10.4209/aaqr.2014.08.0166

Deposition Removal of Monodisperse and Polydisperse Submicron Particles by a Negative Air Ionizer

Yi-Ying Wu[#], Yen-Chi Chen[#], Kuo-Pin Yu[*], Yen-Ping Chen, Hui-Chi Shih

Institute of Environmental and Occupational Health Sciences, National Yang-Ming University, No.155, Li-Nong Street, Section 2, Taipei, Taiwan

ABSTRACT

Indoor particulate matter exposure is one of the main environmental risk factors influencing human health. Previous studies have indicated that the degree of hazards about ultrafine particles was associated with the particle surface area and number concentration. Polydisperse submicron particles (PSPs) contribute most of the indoor aerosol particle number and are usually used for removal testing. However, the behaviors of monodisperse submicron particles (MSPs) are easier to analyze. This study aims to investigate the difference between the deposition removal efficiency of MSP and PSP by the negative air ionizer (NAI) under different settings of freestream air velocity (FAV).

The particle-removal experiments were conducted in a stainless steel test chamber under the condition of 50% relative humidity and FAV of 0.56, 1.2 and 2.0 m/s. The NaCl and oleic acid PSPs were generated from a constant output atomizer and the NaCl MSPs (30, 50, 100, 170 and 300 nm) were generated by passing the polydisperse NaCl aerosol through a Differential Mobility Analyzer. The concentration and size distribution of the particles in the chamber were monitored with a Scanning Mobility Particle Sizer (SMPS). The decay constant of particles number concentration, particle removal efficiency (*PRE*), enhancement factor of deposition rate (*EF*) and air cleaner effectiveness (*ACE*) were determined from the SMPS data.

The decay constant of particle number concentration increased with the decrease of FAV and decreased with the increase of particle size. Both of the *PRE*s of MSP and PSP were quite high, especially for the smaller particles and under low FAV. The *EF*s ranged from 4.4 to 115.5 and were proportional to the particle size. In addition, the *ACE* ranged from 0.57 to 0.96 and increased as the particle size increased. These results give a better understanding of the deposition of 30–300-nm particles enhanced by the NAI and the influential factors.

***Keywords*:** Submicron particles; Negative air ionizer; Enhancement factor.

INTRODUCTION

Up to 30 percent of the total burden of diseases was caused by particulate matter (PM) (Morawska *et al.*, 2013), and most of the PM exposure happens in indoor environments where modern people spend most of their time (Klepeis *et al.*, 2001). Thus, indoor PM exposure is one of the main environmental risk factors influencing human health. Ultrafine particles (UFP < 100 nm) have been shown to contribute 19% to 76% of indoor-generated particles (Morawska *et al.*, 2013). The inhalation of UFP can cause numerous adverse health effects on the lungs, including pulmonary fibrosis, pulmonary inflammation, pleural effusion, granuloma, and increase of cancer risk (Song *et al.*, 2009; Wang *et al.*, 2009; Sze-To *et al.*, 2012). The neuronal translocation through nasal tracheobronchial, olfactory and trigeminal nerves and translocation across the blood-brain barrier in certain regions of the brain might serve as pathways for central nerves system exposure to UFPs (Oberdörster *et al.*, 2004). In view of the serious hazards caused by the inhalation of indoor aerosol particles, a focus on exposure control is severely needed.

Many researchers have shown that a negative air ionizer (NAI) can charge the airborne particles and force them to be deposited more rapidly than the uncharged ones due to the electrostatic force (Grabarczyk, 2001; Lee *et al.*, 2004; Mayya *et al.*, 2004; Grinshpun *et al.*, 2005; Wu *et al.*, 2006; Grinshpun *et al.*, 2007; Shiue *et al.*, 2011; Yu, 2012). Many factors have been shown to influence the effectiveness of air ionizer on the deposition of particles, such as particle size and composition, relative humidity, operation time of air ionizer and wall surface materials (Grabarczyk, 2001;

[#] Equal contribution.

[*] Corresponding author.
Tel.:+886-2-28267933; Fax: +886-2-28278254
E-mail address: kpyu@ym.edu.tw

Lee *et al.*, 2004; Mayya*et al.*, 2004; Grinshpun *et al.*, 2005; Wu *et al*., 2006; Grinshpun *et al.*, 2007; Shiue *et al.*, 2011; Yu, 2012). Other factors, including air movement and particle size distribution (monodisperse or polydisperse), may also affect the efficiency of NAI on the deposition removal of particles (Lai and Nazaroff, 2000; Zhao *et al.*, 2004; Zhao and Wu, 2006). Generally, indoor aerosol particles are polydispersely distributed. However, the behavior of monodisperse particles is simpler and more easily proven by the theoretical model. There were rare researches on the deposition removal of monodisperse submicron particles (MSPs), with the enhancement of NAI. Understanding the difference between the deposition removal of MSPs and polydisperse submicron particles (PSPs), which has become an urgent work, can help us apply the theoretical model in the real situation.

The objective of this study is to investigate the effects of particle size distribution (MSPs and PSPs), the freestream air velocity (FAV) and particle composition (NaCl and oleic acid), on the particle deposition enhanced by the NAI. The particle sizes of 30–300 nm were targeted because most of pathogenic viruses, commonly used nano materials, and the most penetrating particle size of filters fall within these size ranges. Many previous studies have indicated that the degree of hazards about fine and ultrafine particles was associated with the particle number rather than particle mass (Donaldson *et al.*, 1998; Oberdörster *et al.*, 2005; Grass *et al.*, 2010). Therefore, the particle removal focuses on the number concentration rather than the particle mass concentration. The result of this study can help establish a better understanding of the deposition of 30–300 nm particles enhanced by the NAI and the influential factors.

METHODOLOGIES

Experiment System

The schematic diagram of the experimental setup is shown in Fig. 1. In this setup, the zero air supply system which is composed with oil-free air compressor, diffusion dryer and active carbon and HEPA filter offered the clean air for the polished stainless steel cubic test chamber (60 cm × 60 cm × 60 cm). The relative humidity (RH) of the chamber air was maintained at 50% ± 3% by controlling the ratio of saturated air flow rate to dry air flow rate with a pair of mass flow controllers (MFCs). To investigate the effect of freestream air velocity on the deposition removal of particles, the experiments were conducted in the test chamber with a metal fan providing freestream air velocity of 0.56, 1.2 and 2.0 m/s (were defined as low, medium and high freestream air velocities). These air velocities approximately cover the range for mechanically ventilated indoor space and the ventilation duct (Lai and Nazaroff, 2000). The freestream air velocity, temperature, RH and CO_2 concentrations of the chamber air were recorded by the indoor air quality monitor (Q-Trak 7565-X, TSI Inc.) every one minute. The air velocity patterns in the chamber under various freestream

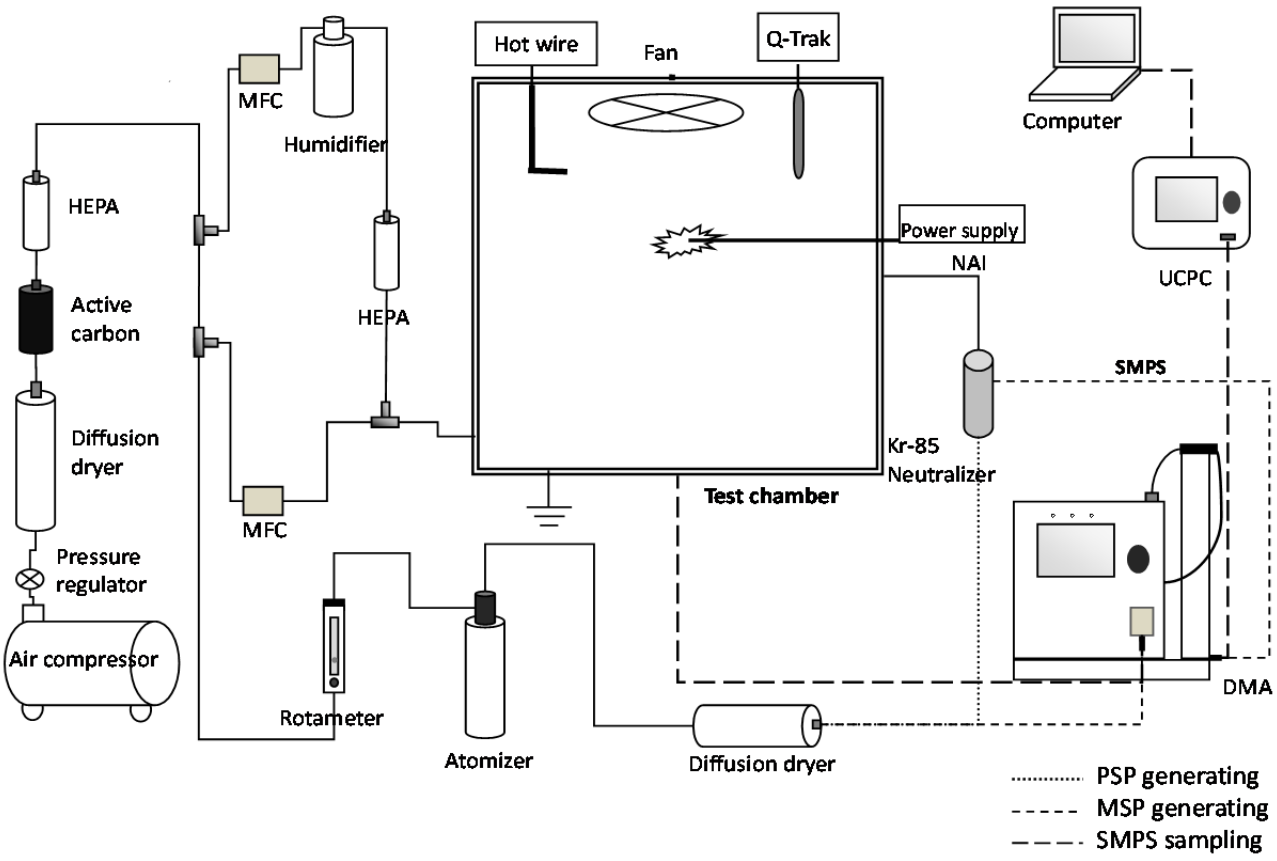

Fig. 1. Experimental setup.

air velocities are shown in Fig.2. The air moved very fast to various directions and mixed well in the center of the chamber (mixing level > 95%). However, the air flow rate is much slow near the surface of the chamber wall. And the air flow patterns agree with the widely accepted description that there are three zones in a turbulent boundary layer (Lai and Nazaroff, 2000).

Both PSPs and MSPs were employed in the particle-removal experiments to investigate the effect of particle size distribution on the deposition removal of particles. The PSPs were generated from a Collison-type constant output atomizer (Model 3076, TSI Inc. USA). According to the electrical mobility of particles, the MSPs with size of 30, 50, 100, 170 and 300 nm were generated by passing the polydisperse aerosols through a Differential Mobility Analyzer (DMA, Model 3081, TSI Inc., USA). All the generated particles were neutralized by the Kr-85 radioactive Aerosol Neutralizer (Model 3077, TSI Inc., USA) before entering the chamber. To examine the effect of aerosol particles' relative permittivity on the deposition removal of particles enhanced by an operating NAI, we selected two kinds of aerosol particles: NaCl (relative permittivity = 6.1) and oleic acid (relative permittivity = 2.5) to conduct the particle-removal experiments.

In the particle-removal experiments, the aerosol particle number concentration and size distribution in the test chamber were monitored in real time by the Scanning Mobility Particle Sizer (SMPS, Model 3936L76, TSI Inc., USA). A commercial NAI (STR-11, Rayuan Co. Ltd.) with a carbon fiber emission source was used for testing. The concentration of negative air ion and strength of electrostatic field generated by the NAI were measured by an Air Ion Counter (AIC-20M, Alpha Lab, Inc. USA) and an Electrostatic Field Meter (EFM 231, Kleinwächter Ltd.), respectively.

Before each experiment got started, we would clean up the aerosol particles in the chamber by purging the chamber with zero air and operating the NAI for about half an hour, until the aerosol particle number concentration in the chamber reduced to less than 100 particles/cm^3. After each experiment, we would clean up the chamber wall with 75% ethanol.

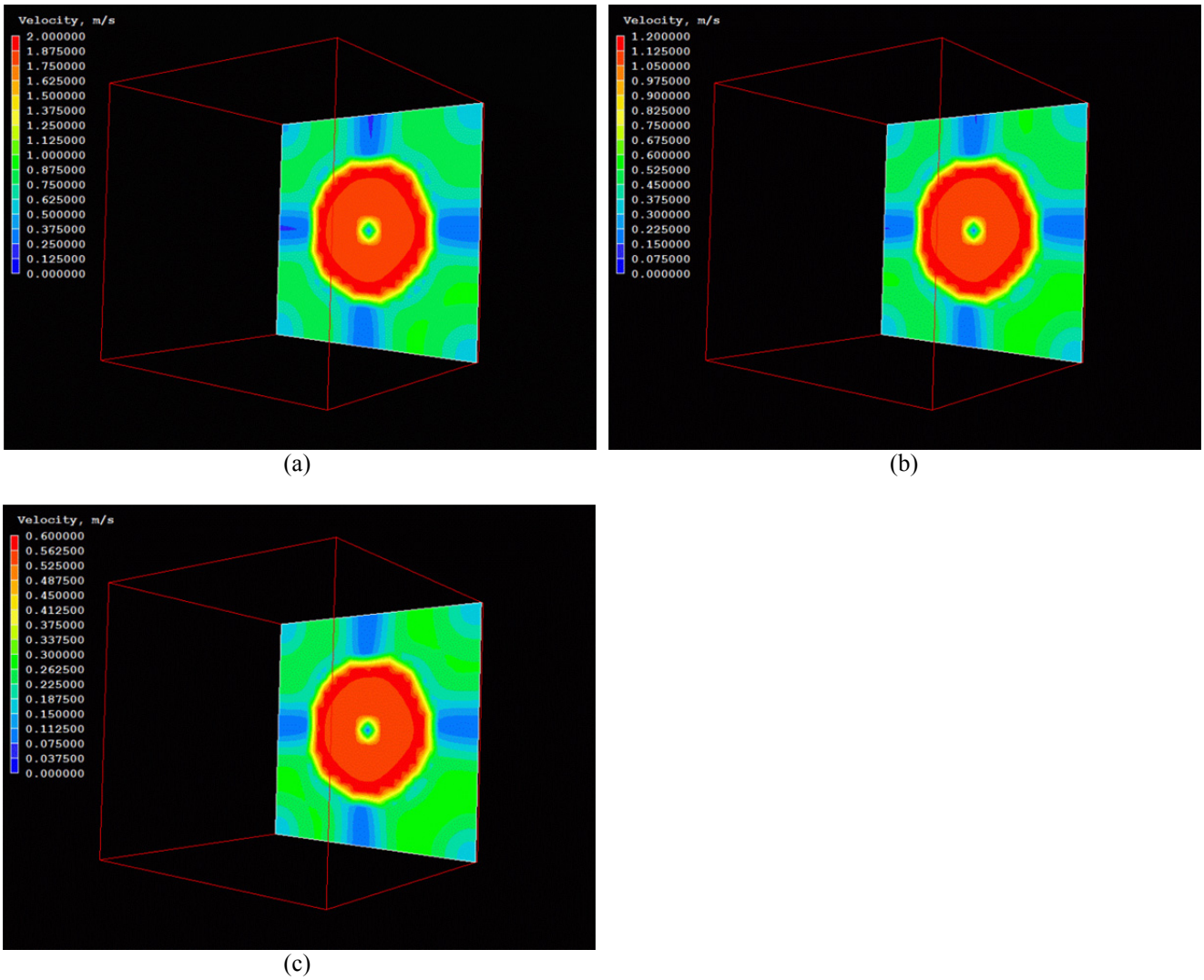

Fig. 2. Air velocity patterns in the chamber (a) high freestream air velocity (b) medium freestream air velocity (c) low freestream air velocity.

Parameter Determined

In this study, the Particle Concentration Fraction (*PCF*), Particle Removal Efficiency (*PRE*), Decay Constant (*k*), Enhancement Factor of deposition rate (*EF*) and Air Cleaner Effectiveness (*ACE*) of removal rate were determined from the time profiles of the particle number concentration and size distribution. The *PCF* and *PRE* are expressed as:

$$PCF = \frac{C\left(d_p, t\right)}{C\left(d_p, t=0\right)} = 1 - PRE \tag{1}$$

where $C(d_p,t)$ is the number concentration of aerosol particles with diameter d_p at time t; $C(d_p, t = 0)$ is the number concentration of aerosol particles with diameter d_p when $t = 0$.

The decay constant of aerosol particle number concentration is defined as what follows:

$$C\left(d_p, t\right) = C\left(d_p, t=0\right) \times e^{-kt} \tag{2}$$

where k is the decay constant. From the experiment, two decay constants were obtained: the natural decay constant (k_n) which represents the decay rate constant of aerosol particle number concentration with no NAI operating, and the decay constant (k_a) which represents the decay rate constant of aerosol particle number concentration with an operating NAI.

Enhancement factor, *EF*, is defined as the ratio of the effective decay rate constant of aerosol particle number concentration with an operating NAI to that without any NAI operating and this parameter represents the net effectiveness of NAI. *EF* is given by:

$$EF = \frac{k_a - \lambda_a}{k_n - \lambda_n} \tag{3}$$

where k is the decay constant of particles; λ is the air change per hour; the subscripts a and n denote the conditions with an NAI and with no NAI operating, correspondingly.

Air cleaner effectiveness (*ACE*) of the NAI for the removal of aerosol particles in the test chamber is expressed as what follows (Waring *et al.*, 2008):

$$ACE = 1 - \frac{\lambda_n + \beta}{\lambda_n + \beta + ECR/V} \tag{4}$$

in which, β is the particle deposition loss-rate coefficient; V is the volume of test chamber; *ECR* is the effective clean rate [$ECR = (k_a - k_n)V$].

Statistical Method

The data size is small [replica for each data point (n = 3); particle sizes (n = 5), combined (n = 15)], and the type of data distribution is not a normal distribution. Thus, the correlations between various parameters and factors were tested with the nonparametric method (Spearman's rho) by using the SPSS Statistics 17 Software.

RESULTS AND DISCUSSION

Natural Decay of Aerosol Particle Concentrations

In this study, the "natural decay" of aerosol particle represents the particle loss due to ventilation and deposition onto the chamber wall without any NAI operating. Because all the tested aerosol particles in this study were smaller than 0.5 μm, the inertial drift was assumed to be a minor factor for particle deposition. The Brownian diffusion and turbulent diffusion are the two mechanisms governing the particle transport through the boundary layer to the chamber wall.

Table 1 shows the particle removal efficiency (*PRE*) at various time points under different conditions. In general, smaller particles have higher removal efficiency. Besides, increasing freestream air velocity can enhance the removal efficiency of NaCl MSP. However, there seems to be no obvious impact of the freestream air velocity on the removal efficiency of PSP.

In the NaCl MSP deposition experiments, there was no observable coagulation between particles. On the other hand, the polydisperse coagulation coefficient is larger than the monodisperse ones and it increased rapidly when the ratio of the particle sizes increased as shown in Fig. 3. Additionally, the initial number concentrations of PSP were higher than 10^5 particles/cm^3. Thus, particle coagulation occurred in the natural decay experiments of PSP as demonstrated in Fig. 4. The PSP coagulation led to a higher initial number-concentration decay rate as compared to that of MSP (Fig. 5). However, when the particle number concentration reduced to $< 10^5$ particle/cm^3, the natural number-concentration decay rate of PSP would slow down and the decay rate constant of PSP would become similar to the decay constants of MSP, as shown in Figs. 4(a) and 4(b) and Figs. 5(a)–5(c). Although the coagulation of particles can reduce the particle number concentration, the coagulated particles were still suspended in the air and would still cause inhalation exposure.

Effect of Freestream Air Velocity and Particle Size on Natural Decay Rate

As demonstrated in Fig. 6, the natural decay constants of aerosol number concentration (k_n) increased with the increase of freestream air velocity. This result was associated with the friction velocity (u^*) which directly affected the particle transport from the region outside the boundary layer toward the chamber wall. For particles smaller than 0.5 μm, the deposition loss-rate coefficient (β) increased as the friction velocity increased. Friction velocity can be expressed as what follows (Lai and Nazaroff, 2000):

$$u^* = \sqrt{\frac{\tau_w}{\rho_a}} \tag{5}$$

in which ρ_a is the density of air; τ_w is the shear stress at thechamber wall and can be expressed as the following equation (Lai and Nazaroff, 2000):

$$\tau_w = \rho_a \gamma \frac{dU}{dy}\Big|_{y=0} \tag{6}$$

Table 1. Particle removal efficiency (PRE %) at various time points and under different conditions.

Condition	Low freestream air velocity										Medium freestream air velocity										High freestream air velocity									
	Natural decay					NAI					Natural decay					NAI					Natural decay					NAI				
NaCl MSP																														
Time (min)	30 nm	50 nm	100 nm	170 nm	300 nm	30 nm	50 nm	100 nm	170 nm	300 nm	30 nm	50 nm	100 nm	170 nm	300 nm	30 nm	50 nm	100 nm	170 nm	300 nm	30 nm	50 nm	100 nm	170 nm	300 nm	30 nm	50 nm	100 nm	170 nm	300 nm
3	6.8	19.1	10.7	12.0	10.7	95.5	92.2	80.9	74.4	59.1	22.4	10.1	6.1	6.5	8.1	96.0	89.7	81.9	75.0	68.1	32.2	18.3	8.6	14.0	17.2	88.3	76.2	58.6	50.7	43.6
6	30.3	25.9	12.4	11.7	27.6	**100**	99.7	97.2	93.8	86.6	36.1	28.1	10.7	25.8	8.4	99.2	99.9	96.7	95.9	85.8	59.9	35.9	14.3	13.6	32.5	99.5	96.8	84.3	82.6	76.3
9	40.3	25.0	20.8	18.5	32.7		**100**	99.5	97.8	96.0	51.1	34.0	22.1	28.9	12.3	**100**	**100**	99.1	97.2	93.9	67.3	46.4	31.0	26.2	33.7	**100**	99.4	95.2	94.0	90.9
15	55.9	42.0	28.1	31.9	41.0			**100**	**100**	**100**	70.7	53.9	36.4	38.2	24.5			**100**	**100**	**100**	85.2	65.3	36.7	34.3	39.6		**100**	99.7	98.7	98.5
24	75.1	59.2	44.5	35.4	57.5						88.0	70.9	49.9	56.0	26.0						94.2	82.8	58.6	50.8	45.8			**100**	**100**	**100**
NaCl PSP																														
Time (min)	30 nm	50 nm	100 nm	170 nm	300 nm	30 nm	50 nm	100 nm	170 nm	300 nm	30 nm	50 nm	100 nm	170 nm	300 nm	30 nm	50 nm	100 nm	170 nm	300 nm	30 nm	50 nm	100 nm	170 nm	300 nm	30 nm	50 nm	100 nm	170 nm	300 nm
3	49.6	27.7	11.6	12.1	6.1	97.5	93.4	82.7	76.1	71.0	34.1	21.3	13.3	11.3	6.7	97.9	94.0	82.7	76.4	70.8	49.3	30.8	15.8	13.9	1.2	97.6	94.2	85.3	80.0	73.9
6	70.5	48.6	22.2	18.6	9.0	**100**	99.6	97.5	94.9	92.6	53.4	39.7	24.1	19.5	8.2	**100**	99.8	97.3	94.9	92.0	74.4	51.9	30.6	22.8	16.5	99.6	99.8	98.6	95.6	92.0
9	86.0	61.6	33.2	23.3	18.3		**100**	99.5	98.7	98.0	78.2	54.1	30.8	24.7	16.5		**100**	99.5	98.8	97.7	87.0	65.3	40.6	31.2	22.9	**100**	**100**	99.7	99.2	98.4
15	93.0	74.3	45.1	33.2	21.0			**100**	99.9	99.8	88.7	71.0	46.5	36.6	24.1			**100**	**100**	**100**	94.3	78.9	53.2	41.7	33.3			**100**	**100**	99.8
24	98.3	86.7	59.5	46.9	26.8				**100**	**100**	96.3	83.3	60.8	49.7	35.4						98.6	91.1	66.5	55.4	44.7					**100**
Oleic acid PSP																														
Time (min)	30 nm	50 nm	100 nm	170 nm	300 nm	30 nm	50 nm	100 nm	170 nm	300 nm	30 nm	50 nm	100 nm	170 nm	300 nm	30 nm	50 nm	100 nm	170 nm	300 nm	30 nm	50 nm	100 nm	170 nm	300 nm	30 nm	50 nm	100 nm	170 nm	300 nm
3	55.3	33.1	17.0	9.6	2.9	93.8	87.4	76.9	72.6	69.7	51.2	32.9	17.3	10.1	2.3	96.0	89.7	78.4	72.5	67.8	67.8	43.4	23.5	10.6	8.5	95.9	89.8	78.6	73.0	68.6
6	75.6	53.8	29.3	18.1	5.5	99.6	98.8	95.5	93.9	92.2	74.6	50.9	30.5	20.0	11.1	99.5	99.0	95.5	92.9	89.7	84.1	67.2	41.0	22.6	11.9	99.0	99.0	95.6	92.8	90.9
9	87.2	66.6	39.4	25.1	10.7	99.9	99.8	99.0	98.6	98.3	87.1	64.6	41.5	26.9	11.6	99.8	99.8	98.9	98.1	96.8	94.7	79.8	50.7	33.4	17.7	99.7	99.8	98.8	97.9	96.9
15	93.9	80.9	52.4	36.9	14.7	**100**	**100**	**100**	99.9	99.8	95.2	79.4	54.5	40.8	21.3	**100**	**100**	99.9	99.9	99.8	98.9	90.0	66.8	47.4	29.7	**100**	**100**	99.9	99.8	99.6
24	98.3	89.2	66.4	51.3	30.5				**100**	**100**	97.8	89.7	67.8	55.5	36.3			**100**	**100**	**100**	99.5	96.4	79.0	61.8	44.8			**100**	**100**	**100**

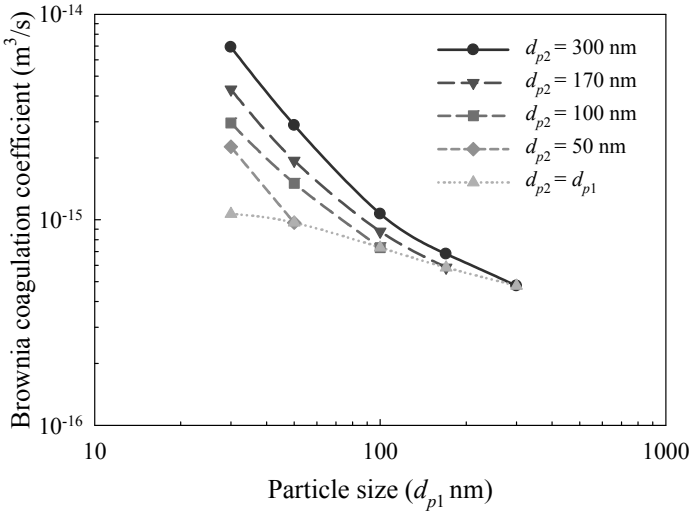

Fig. 3. Brownia coagulation coefficient $K_{1,2}$ for coagualtion of particles of diameters d_{p1} and d_{p2}.

$$K_{1,2} = \pi(d_{p1}D_{p1} + d_{p1}D_{p2} + d_{p2}D_{p1} + d_{p2}D_{p2})$$

$$D_{p1} = kTB = \frac{kTC_c}{3\pi\eta d_{p1}}$$

D_{p1} is the diffusion coefficient of particle with diameter of d_{p1}; k is the Boltzmann constant (1.38×10^{-23} J/K); T is absolute temperature; B is the mechanical mobility of particle with diameter of d_{p1}; C_c is Cunningham slip correction factor; η is the viscosity of air.

where, γ is the kinematic viscosity of air; U is the time-averaged air velocity parallel to the chamber wall surface; y is the distance from the chamber wall surface. The average velocity gradient is a function of freestream air velocity (U_∞) (Lai and Nazaroff, 2000):

$$\frac{dU}{dy}|_{y=0} = \left(\frac{0.074}{\rho_a \gamma}\right)\left(\frac{\rho_a U_\infty^2}{2}\right)\left(\frac{U_\infty L}{\gamma}\right)^{-1/5} \quad (7)$$

in which L is a characteristic length of chamber surface. Substituting Eq. (7) into Eq. (6), and then substituting the resulting equation into Eq. (5), we have the friction velocity:

$$u^* = \sqrt{\left(\frac{0.074}{\rho_a}\right)\left(\frac{\rho_a U_\infty^2}{2}\right)\left(\frac{U_\infty L}{\gamma}\right)^{-1/5}} \propto U_\infty^{9/10} \quad (8)$$

According to Eq. (8), the friction velocity is proportional to the 9/10 power of freestream air velocity and in this study we employed the mean air speed (wind speed) to represent the freestream air velocity. We employed the Lai and Nazaroff'smodel (Lai and Nazaroff, 2000) to estimate the deposition loss-rate coefficient (β) of particle concentration:

$$\beta = \frac{v_{dv}A_v + v_{du}A_u + v_{dd}A_d}{V} \quad (9)$$

where A_v, A_u and A_d are the areas of vertical, upward-facing and downward-facing surfaces, respectively; V is the volume of test chamber. The parameters v_{dv}, v_{du} and v_{dd} are the deposition velocities of particles on vertical surface, upward horizontal surface and downward horizontal surface, respectively. The estimations of v_{dv}, v_{du} and v_{dd} were described with details in Lai and Nazaroff's study (2000). In this model, the friction velocity and particle size are the two major factors that determine the deposition rate of particle toward the surface of chamber wall.

The theory of Lai and Nazaroff's deposition model is based on the understanding that there is a thin particle-concentration boundary layer within the turbulent boundary layer above a wall surface. Because the air velocity is low, no particle rebound or resuspension is considered (the surface is a perfect sink for particles). There is no source or sink of particle with the boundary layer. Thus, the particle flux, J, is constant through the concentration boundary layer and is described by a modified form of Fick's first law:

$$J = -(D + \varepsilon_p)\frac{\partial C}{\partial y} - iv_s C \quad (10)$$

in which D is the Brownian diffusivity of the particles; ε_p is the particle eddy diffusivity; C is the particle number concentration in air; y is the distance from the chamber wall surface; v_s is the gravitational settling velocity of particles. The terms on the right-hand side of Eq. (10), stand for the Brownian and eddy diffusion, and gravitational settling, respectively. The orientations of deposition surface as vertical, upward-facing (floor), or downward-facing (ceiling) are presented in the term i as 0, 1, or –1, respectively (Lai

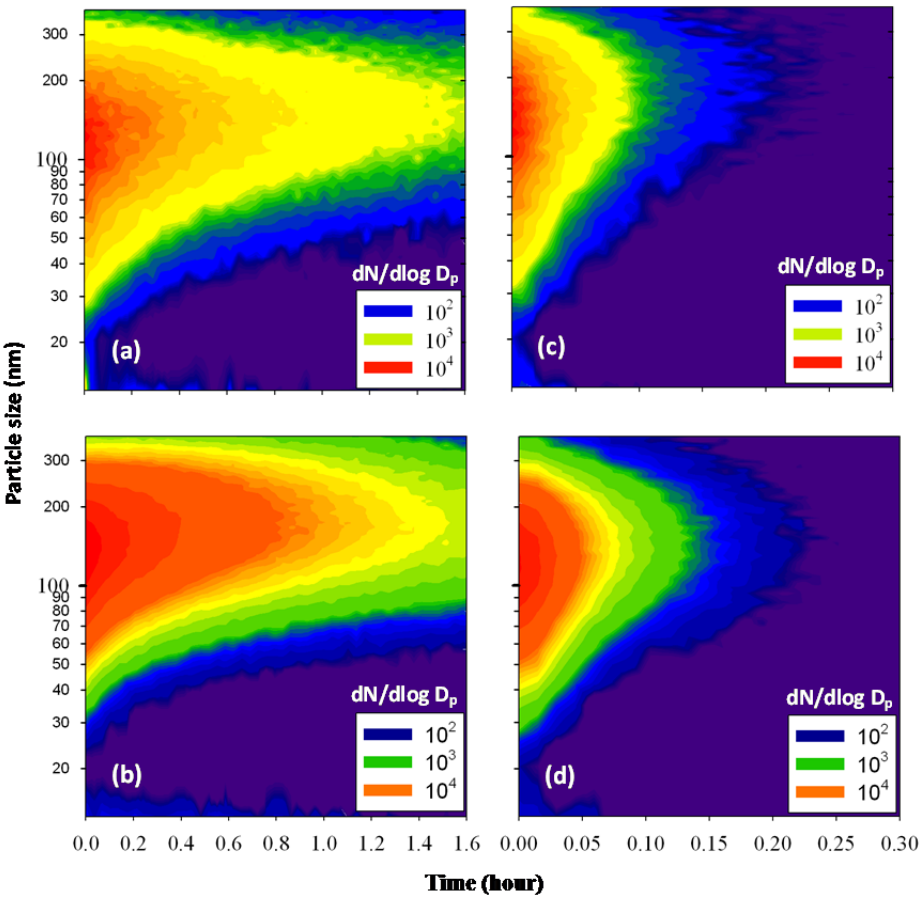

Fig. 4. The time profile of PSP size distribution and concentration under low freestream air velocity (a)(b) NAI off; (c)(d) NAI on; (a)(c) NaCl PSP; (b)(d) Oleic acid PSP.

and Nazaroff, 2000). There is another assumption required for Eq. (10) to be valid: the air in the chamber is well mixed so that the particle-concentration gradient exists only very close to the deposition surface. In Lai and Nazaroff's model, the particle-concentration boundary layer is treated as three sublayers when defining the dependence of particle eddy diffusivity (ε_p) on air turbulent viscosity (ν_t), and the wall effect is also considered.

The summation of β and air exchange per hour (λ) under different friction velocity is illustrated in Fig. 6. The trends of these curves ($\beta + \lambda$) are consistent with the natural decay constants of number concentration (k_n). The k_n is negatively correlated with the particle size as shown in Fig. 7 and the correlation coefficients are shown in Table 2. This is owing to the larger particles possess higher inertia and does not repond to the turbulent fluctuations of air flow as well as smaller particles. Thus, the eddy diffusivity of larger particles in the boundary layer is lower than those of smaller ones. Consquently, larger particles deposit slower than smaller ones.

Enhancement Effect of NAI on the Deposition of Aerosol Particles

As shown in Table 1, there were still 0.5% to 76% of particles suspended in the chamber air after 24-minute "natural decay." However, the particles were totally removed within 6–24 minutes after the NAI started operating, indicating a powerful enhancement effect of NAI on the deposition of aerosol particles. When the NAI was operating, an electric field would be generated, and the aerosol particles would be charged by the negative air ion clusters. The number of charges obtained [$n_d(t)$] by a particle by diffusion charging in a period of time t can be estimated by the following equation (Hinds, 1999):

$$n_d(t) = \frac{d_p bT}{2K_E e^2} \ln\left[1 + \frac{\pi K_E d_p \bar{c}_i e^2 N_i t}{2bT}\right] \quad (10)$$

in which d_p is the particle diameter; T is the absolute temperature; b is the Boltzmann constant (1.38×10^{-23} J/K); K_E is a constant (9.0×10^9 N m^2/Coulomb^2); e is the electronic charge (1.6×10^{-19} Coulomb); N_i is the concentration of negative air ion generated by the NAI, and c_i is the mean thermal speed of ions (240 m/s). The number of charges [$n_f(t)$] acquired by a particle via field charging during a period of time t is (Hinds, 1999):

$$n_f(t) = \left(\frac{3p}{p+2}\right)\left(\frac{Ed_p^2}{4K_E e}\right)\left(\frac{\pi K_E e Z_i N_i t}{1 + \pi K_E e Z_i N_i t}\right) \quad (11)$$

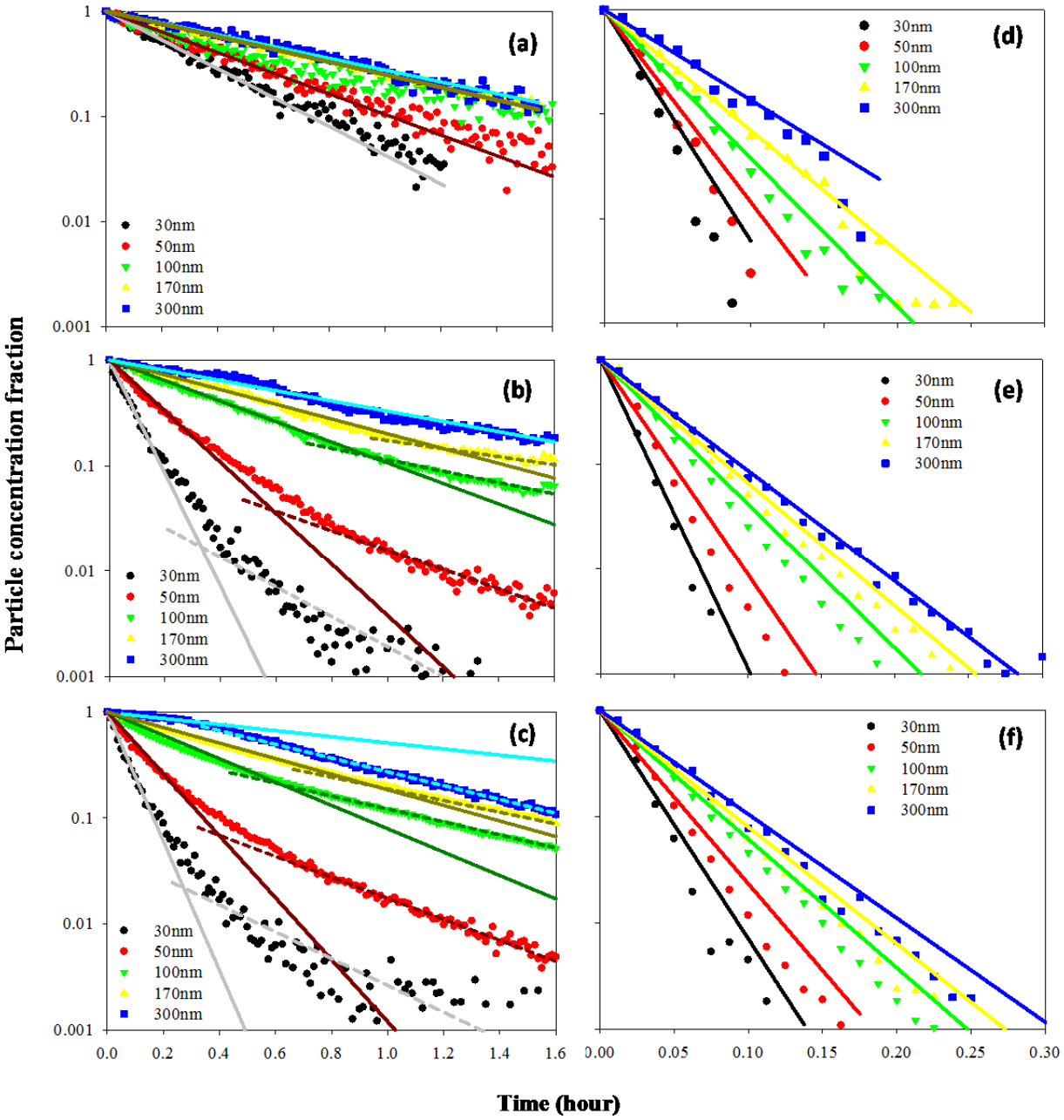

Fig. 5. The time profile of (a)(d)NaCl MSP; (b)(e) NaCl PSP; (c)(f) Oleic acid PSP number concentrations under low freestream air velocity (a)(b)(c) NAI off; (d)(e)(f) NAI on; the short dash fitting curves in (b) and (c) have similar slopes to the corresponding fitting curves in (a), indicating that the decay rate is similar.

where p is the relative permittivity of the particle; E is the electric field strength; Z_i is the mobility of negative air ions (approximately 0.00015 $m^2/V \cdot s$). The terminal electrostatic velocity (v_{TE}) of a particle carrying $[n_d(t) + n_f(t)]$ charges in an electric field is (Hinds, 1999):

$$v_{TE} = EZ_p = \frac{EeC_c}{3\pi\eta d_p}[n_d(t) + n_f(t)] \quad (12)$$

where Z_p is the particle electric mobility; C_c is the Cunningham slip correction factor; η is viscosity of the air. By measuring the N_i and E generated by the NAI and using Eq. (12), we have the v_{TE}, and the particle deposition loss-rate coefficient (β_{NAI}) is:

$$\beta_{NAI} = \frac{(v_{dv} + v_{TE})A_v + (v_{du} + v_{TE})A_u + (v_{dd} + v_{TE})A_d}{V} \quad (13)$$

Eq. (13), which includes the effect of NAI on particle deposition, is analogous to Eq. (9). Fig. 6 demonstrates that the particle-size-dependent trend of $\beta_{NAI} + \lambda$ is similar to that of k_a. Moreover, increasing freestream air velocity would reduce the concentration of negative air ions and electric field strength generated by the operating NAI,

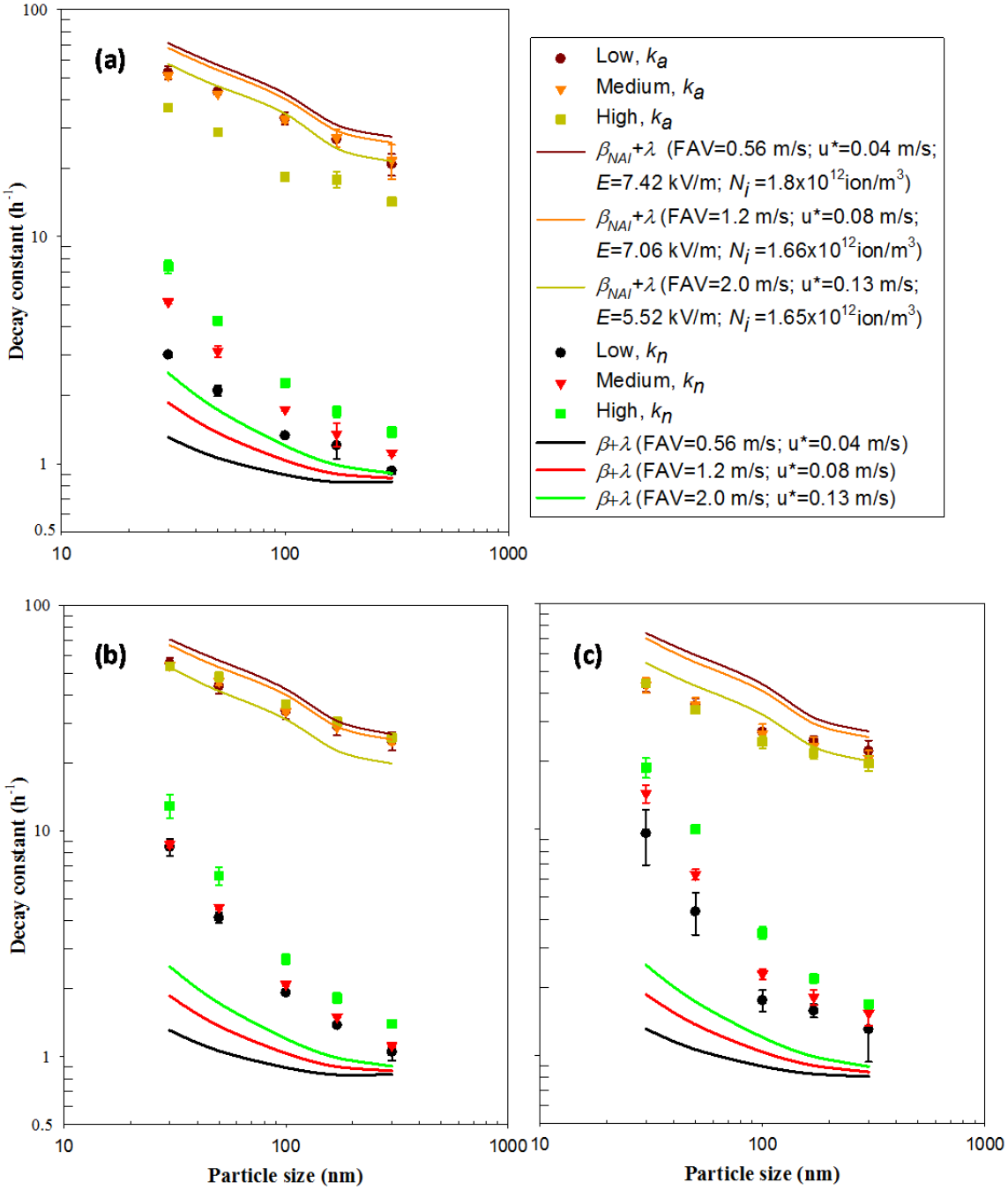

Fig. 6. The relationship between decay constants and particle sizes under various friction velocities (a) NaCl MSP (b) NaCl PSP (c) Oleic acid PSP. FAV: freestream air velocity.

resulting in the decrease of the terminal electrostatic velocity of the particles. Thus, k_a in "high" freestream air velocity was significantly lower than that in "low" and "medium" freestream air velocity.

Enhancement Factor of Particle Deposition Rate

The enhancement factor of particle deposition rate (*EF*) is the β_{NAI}/β ratio, indicating that how many folds of particle deposition rate was increased by the operating NAI. As shown in Fig. 7, the *EF* is propotional to the particle size and ranges from 2.4 to 115.5, and the correlation coefficients are listed in Table 2. Increasing freestream air velocity would reduce the negative air ion concentration and electric field strength generated by the operating NAI, and would make the *EF* decrease. However, the effect of freestream air velocity on the *EF* of PSP was not as significant as *EF* of MSP. Kinematic coagulation of PSP driven by airflow might be one of the reasons to this phenomenon. Although increasing freestream air velocity would decrease the enhancement effect of NAI on the particle deposition. It enhanced the kinematic coagulation of PSP, which impaired the apparent impact of freestream air velocity on the *EF*. In

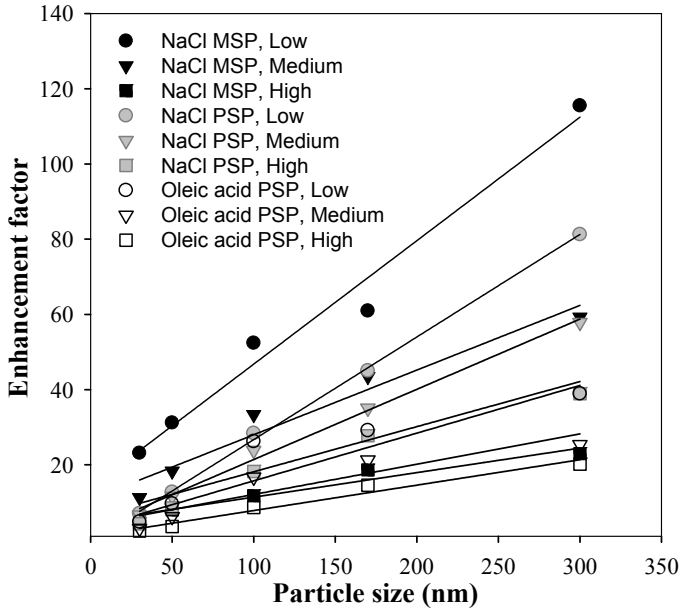

Fig. 7. The relationship between EF and particle size (diameter) under various freestream air velocities (Low, Medium and High).

Table 2. The correlation coefficients (Spearman's rho) between particle size and various parameters under different experimental conditions.

Parameter / Condition	k_n *vs.* d_p *(n = 15)*	k_a *vs.* d_p *(n = 15)*	*EF vs.* d_p *(n = 5)*
NaCl MSP, Low	–0.945**	–0.981**	0.999**
NaCl MSP, Medium	–0.981**	–0.968**	0.999**
NaCl MSP, High	–0.981**	–0.928**	0.999**
NaCl PSP, Low	–0.985**	–0.956**	0.999**
NaCl PSP, Medium	–0.981**	–0.941**	0.999**
NaCl PSP, High	–0.949**	–0.981**	0.999**
Oleic acid PSP, Low	–0.919**	–0.829**	0.999**
Oleic acid PSP, Medium	–0.949**	–0.895**	0.999**
Oleic acid PSP, High	–0.982**	–0.865**	0.999**

addition, the particle electric mobility Z_p is positively correlated to the particle diameter d_p (Hinds, 1999):

$$Z_p = \frac{v_{TE}}{E} = \frac{C_c}{6\pi K_E \eta}\left[\frac{kT}{e}\ln\left(1+\frac{\pi K_E d_p \bar{c}_i e^2 N_i t}{2bT}\right) + \left(\frac{3\varepsilon}{\varepsilon+2}\right)\left(\frac{Ed_p}{2}\right)\left(\frac{\pi K_E e Z_i N_i t}{1+\pi K_E e Z_i N_i t}\right)\right] \quad (14)$$

which is consistent with the positive correlation between *EF* and particle diameter as shown in Fig. 7.

The *EF* of oleic acid PSP deposition was lower than that of NaCl PSP and there were some reasons for this result. First, the relative permittivity of NaCl particle is higher than that of oleic acid particle. Therefore, NaCl particles can acquire more charges by field charging, which results in higher terminal electrostatic velocity. However, this effect is insignificant when particles are smaller than 200 nm. Additionally, only a minor fraction in the size distribution of oleic acid PSP was constituted by the particles smaller than 40 nm. In order to obtain an observable level of oleic acid particles smaller than 40 nm and facilitate the measurement of particle deposition, we employed a higher initial concentration of oleic acid PSP as compared to that of NaCl PSP. However, higher number concentration would result in a higher loss rate (higher k_n) due to coagulation and a lower ion/particle ratio, which might reduce the charging efficiency of an operating NAI.

Air Cleaner Effectiveness

The efficiency of NAI on the removal of aerosol particles in a given space may be evaluated by the "air cleaner effectiveness (*ACE*)" (Waring *et al.*, 2008). The *ACE* assumes a well-mixed and steady-state space, is independent of indoor particle source, and is dependent on the volume of the spaces. Waring *et al.* (2008) has demonstrated that *ACE* can be obtained in an unsteady-state chamber by measuring the air exchange per hour of the test chamber (λ), size-resolved particle deposition loss-rate coefficient (β), and clean air

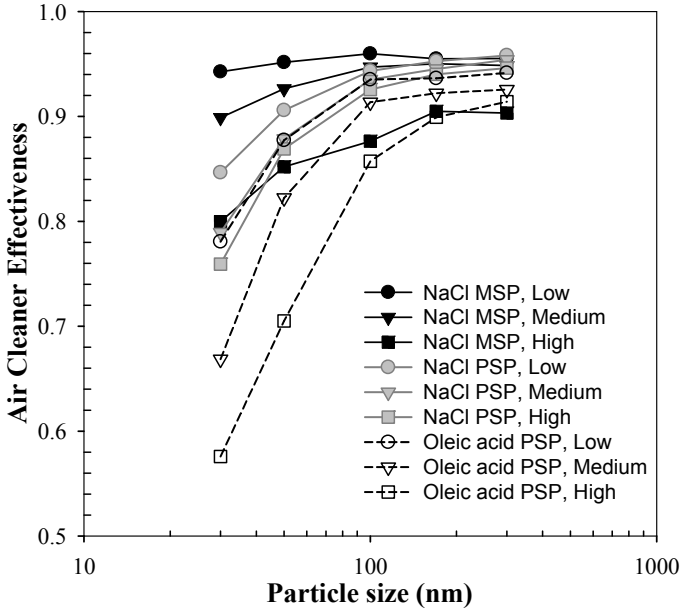

Fig. 8. The relationship between *ACE* and particle size under different freestream air velocities (Low, Medium and High).

delivery rate [$CADR = (k_a - k_n)V$] instead of measuring the steady-state particle concentration:

$$ACE = 1 - \frac{C_{AC}}{C_{No\ AC}} = 1 - \frac{\lambda + \beta}{\lambda + \beta + CADR/V} = 1 - \frac{k_n}{k_a} \quad (15)$$

where C_{AC} and $C_{No\,AC}$ is the steady-state particle concentrations with and without an operating air cleaner, respectively. The air cleaner effectiveness ranges between 0% and 100%, which indicates the removal percentage of the particles. As shown in Fig. 8, the NAI's air cleaner effectiveness for particles larger than 100 nm was higher than 85%. However, the NAI was inefficient for the removal of oleic acid PSP of size smaller than 50 nm ($ACE < 70\%$). The well-mixed space assumption and the dependence of the space volume are the two major considerations when the air cleaner effectiveness of this study is applied in real environments.

In general, our result of air cleaner effectiveness (*ACE* = 0.58–0.96) is comparable to previous studies as demonstrated in Table 3. Both Grinshpun's (Lee *et al.*, 2004; Grinshpun *et al.*, 2005) and Hu's groups (Shiue *et al.*, 2011) found that *ACE* increased with the operation time of NAI. And we also found that the concentration of negative air ions would increase with the operation time of NAI. Our conclusion that in the testing range (30–300 nm particles) the *ACE* for larger particles is better than that for smaller particles is consistent with the result of Wu *et al.* (2006).

Implication in Indoor Environments

The concentration of negative air ion and electric field strength generated by the NAI decreased significantly with the distance away from the NAI (Yu, 2012). Thus, the effectiveness of NAI on the deposition removal of aerosol particles decreased considerably with the increase of room size and the distance between the NAI and wall. A poor performance could be expected, when the NAI is applied in a large room whose volume is much larger than that of the test chamber. However, a meticulous design, including an air cleaner equipped with an NAI and a deposition chamber, or application of NAI in the metal duct of a ventilation system, or using NAI in a confined indoor space such as a car or a cabin (Grinshpun *et al.*, 2005), could help the NAI to achieve its better performance. Besides, there is a lower aerosol particle concentration in normal indoor environments than in our test chamber. Thus, a higher ion/particle ratio could be found in the indoor environments when applying the NAI, and this condition could be beneficial to the performance of NAI. The criterion for the efficient operation of NAI presents as what follows:

$v_{TE} >> v_{dv}$, v_{du} and v_{dd}; that is $v_{TE} \geq 10 \times v_{dv}$, v_{du} and v_{dd}.

In most cases in indoor environments, $v_{du} > v_{dv}$ and v_{dd}, and thus, the criterion becomes $v_{TE} \geq 10 \times v_{du}$. However, the relationships between ion concentration, v_{TE} (Eq. (12)) and v_{du} are complicated:

$$v_{TE} \geq 10 v_{du} = \frac{10 v_s}{1 - \exp\left(-\frac{v_s I}{u*}\right)} \quad (16)$$

in which *I* is the Integral (Lai and Nazaroff, 2000). A practical method is to set a typical v_{du} value (1×10^{-5}–1.2×10^{-4} m/s in this study) first, and then to calculate the corresponding concentration of ions ($N_i t > 3 \times 10^{14}$ ion sec/m^3; the value of *t* was assumed to be $1/k_a$ = 70–250 seconds. And the concentration of ions was 1.2–4.28 $\times 10^{12}$ ion/m^3). Typical indoor particle concentration level ranged from 1×10^9 to 6×10^9 particles/m^3, and thus the expected ion/particle ratio for rooms with the NAI operating is 200–4280.

Table 3. Brief comparison of *ACE* between this study and previous studies.

Reference	This study	Yu, 2012	Shiue *et al.*, 2011	Waring *et al.*, 2008	Grinshpun *et al.*, 2007	Wu *et al.*, 2006	Grinshpun *et al.*, 2005	Lee *et al.*, 2004	Grabarczyk, 2001
Chamber volume (m^3)	0.216	0.216	1.86	14.75	24.3	1	2.6	24.3	50
Ion concentration (ions/m^3)	1.65–1.8 × 10^{12} (negative ions)	3.6–7.7 × 10^{11} (negative ions)	6 × 10^{11} (negative ions)	--	--	3–5 × 10^{9} (negative ions)	5 × 10^{10}~ 3 × 10^{12} (positive or negative ions)	3.6 × 10^{11}– 1.34 × 10^{12} (positive or negative ions)	3.6 × 10^{10}– 1.8 × 10^{12}
Test particles	30–400 nm NaCl and Oleic acid particles	45–191 nm secondary organic aerosols	100–500 nm polystyrene latex sphere	12.6–514 nm (burned incense)	0.04–1.99 μm Smoke and NaCl particles	30 nm, 300 nm NaCl particles	0.35–2.5 μm NaCl particles	0.045–2 μm NaCl particles	0.3–2.5 μm dust
Operation time (min)	> 24	>18	60–300	> 12	120	30	90	15, 30, 60	456
ACE	0.58–0.96	0.87–0.96	0.12–0.87	0.52–0.98	0.61–0.929	0.61–0.87	Initial ACE = 0 > 0.8 after 30-min operation	0.16–0.85 (15-min operation) 0.44–0.97 (30-min operation)	0.95–0.98
Description		*ACE* increases with the increase of relative humidity	*ACE* increases with operation time, but is negative correlated with the particle size	*ACE* decreases with hypothetical room size	*ACE* for smoke particles is better than NaCl particles	*ACE* is highest for stainless steel wall and lowest for cement paint wall. *ACE* for 300-nm particles is better than 30-nm particles	*ACE* increases with the operation time. The effect of particle size, composition of particle on the *ACE* is insignificant	*ACE* increased with the operation time	After 1 h of operating, *ACE* for 0.3–0.4 μm particle is 0.97 and 0.95 for 0.4–2.5 μm particles. *ACE* achieved maximum after 12-h operating.

The conductivity (or relative permittivity, p) of the particles could be another concern when applying the NAI in indoor environments. According to Eq. (11) the relative permittivity of particle materials could affect the number of charges acquired by a particle via field charging. However, the diffusion charging is the predominant mechanism for charging particle smaller than 200 nm (Hinds, 1999). Shin *et al*. (2009) employed three different materials (Ag, $p = \infty$; NaCl, $p = 6.1$; sucrose, $p = 3.3$) to exam the effect of relative permittivity of particle materials on unipolar diffusion charging of submicron particles and found that the material dependence of unipolar diffusion charging for particles ranging from 100 to 200 nm is insignificant. Therefore, even thought the indoor submicron particles cover various relative permittivity, the performance of NAI on the removal of these particles could be similar.

CONCLUSIONS

Because the coagulation coefficient of PSP was larger than that of MSP, the natural decay constant of PSP was higher than that of MSP. In the tested particle size region, the decay constant decreased with the increase of particle size. In contrast, the enhancement factor of particle deposition rate (*EF*)is positively proportional to the particle size. The *EF* of NaCl MSPs was higher than that of NaCl PSPs. By operating an NAI, the deposition rate of particles could be enhanced to as high as 100 times compared to that without any NAI operating. The air cleaner effectiveness (*ACE*) of NaCl MSP under the low freestream air velocity was the highest among all the test conditions and ranged from 94.3% to 96.0%, while the ACE of 30 nm oleic acid particles (PSPs) under high freestream air velocity was the lowest (57.6%) among all the test conditions. Both the *EF* and *ACE* decreased when the freestream air velocity increased.

Conclusively, the NAI performed effectively on enhancing the deposition removal of submicron particles. Although, the interaction between particles and negative air ions in the chamber was complicated and was involved with diffusion, field charging and coagulation, the trend of decay constant measured in the MSP and PSP experiments was corresponding to that predicted by the theoretical model.

ACKNOWLEDGEMENTS

The authors would like to thank the National Science Council of Taiwan for providing the financial support (contract number NSC 100-2221-E-010-003-MY3). We would also like to thank Ms. Jiayu Chen for English editing and Mr. Po-Yu Lin for Computational Fluid Dynamics (CFD) graph.

ABBREVIATION

Air cleaner effectiveness (ACE)
Clean air delivery rate (*CADR*) [$CADR = (k_a - k_n)V$]
Differential Mobility Analyzer (DMA)
Effective clean rate (*ECR)* [$ECR = (k_a - k_n)V$].
Enhancement factor of deposition rate (EF)
Freestream air velocity (FAV; U_∞)
Mass flow controllers (MFCs)
Monodisperse submicron particles (MSPs)
Negative air ionizer (NAI)
Particle removal efficiency (PRE)
Particle Concentration Fraction (PCF)
Particulate matter (PM)
Polydisperse submicron particles (PSPs)
Relative humidity (RH)
Scanning Mobility Particle Sizer (SMPS)

PRINCIPAL SYMBOLS

A_v, $A_u$and A_d: areas of vertical, upward-facing and downward-facing surfaces, respectively
b: Boltzmann constant (1.38×10^{-23} J/K)
β: deposition loss-rate coefficient
c_i: mean thermal speed of ions (240 m/s)
C: particle number concentration in air
$C(d_p,t)$: number concentration of aerosol particles with diameter d_p
C_c: Cunningham slip correction factor
C_{AC} and $C_{No\ AC}$: steady-state particle concentrations with an operating air cleaner and without, respectively
d_p: particle diameter
D: Brownian diffusivity of particle
ε_p: particle eddy diffusivity
e: electronic charge (1.6×10^{-19} Coulomb)
E: electric field strength
η: viscosity of the air
I: the Integral (Lai and Nazaroff, 2000)
k: decay rate constant of aerosol particle number concentration; the subscripts a and n denote the conditions with an NAI and with no NAI operating, correspondingly
K_E: a constant (9.0×10^9 N m^2/Coulomb^2)
L: a characteristic length of chamber surface
λ: air change per hour; the subscripts a and n denote the conditions with an NAI and with no NAI operating, correspondingly
$n_d(t)$: number of charges obtained by a particle by diffusion charging in a period of time t
$n_f(t)$: number of charges acquired by a particle via field charging during a period of time t
N_i: concentration of negative air ion generated by the NAI
p: relative permittivity of the particle
ρ_a: the density of air
γ: the kinematic viscosity of air
u^*: friction velocity
T: absolute temperature
τ_w: the shear stress at the chamber wall
U: the time-averaged air velocity parallel to the chamber wall surface
v_{dv}, v_{du} and v_{dd}: the deposition velocity of particle on vertical surface, upward horizontal surface and downward horizontal surface, respectively
v_s: gravitational settling velocity of particle
v_{TE}: terminal electrostatic velocity of a particle carrying $[n_d(t) + n_f(t)]$ charges in an electric field
V: the volume of test chamber

y: the distance from the chamber wall
Z_i: the mobility of negative air ions (approximately 0.00015 $m^2/V \cdot s$)
Z_p: particle electric mobility

REFERENCES

Donaldson, K., Li, X. and MacNee, W. (1998). Ultrafine (nanometre) Particle Mediated Lung Injury. *J. Aerosol Sci.* 29: 553–560.

Grabarczyk, Z. (2001). Electiveness of Indoor Air Cleaning with Corona Ionizers. *J. Electrostat.* 51–52: 278–283.

Grass, R.N., Limbach, L.K., Athanassiou, E.K. and Stark, W.J. (2010). Exposure of Aerosols and Nanoparticle Dispersions to In Vitro Cell Cultures: A Review on the Dose Relevance of Size, Mass, Surface And Concentration. *J. Aerosol Sci.* 41: 1123–1142.

Grinshpun, S.A., Mainelis, G., Trunov, M., Adhikari, A., Reponen, T. and Willeke, K. (2005). Evaluation of Ionic Air Purifiers for Reducing Aerosol Exposure in Confined Indoor Spaces. *Indoor Air* 15: 235–245.

Grinshpun, S.A., Adhikari, A., Honda, T., Kim, K.Y., Toivola, M., Rao, K.S.R. and Reponen, T. (2007). Control of Aerosol Contaminants in Indoor Air: Combining the Particle Concentration Reduction with Microbial Inactivation. *Environ. Sci. Technol.* 41: 606–612.

Hinds, W.C. (1999). *Aerosol Technology* (Second Edition), John Wiley and Sons, Inc., New York.

Klepeis, N.E., Nelson, W.C., Ott, W.R., Robinson, J.P., Tsang, A.M., Switzer, P., Behar, J.V., Hern, S.C. and Engelmann, W.H. (2001). The National Human Activity Pattern Survey (NHAPS): A Resource for Assessing Exposure to Environmental Pollutants. *J. Exposure Anal. Environ. Epidemiol.* 11: 231–252.

Lai, A.C.K. and Nazaroff, W.W. (2000). Modeling Indoor Particle Deposition from Turbulent Flow onto Smooth Surfaces. *J. Aerosol Sci.* 31: 463–476.

Lee, B.U., Yermakov, M. and Grinshpun, S. (2004). Removal of Fine and Ultrafine Particles from Indoor Air Environments by the Unipolar Ion Emission. *Atmos. Environ.* 38: 4815–4823.

Mayya, Y., Sapra, B., Khan, A. and Sunny, F. (2004). Aerosol Removal by Unipolar Ionization in Indoor Environments. *J. Aerosol Sci.* 35: 923–941.

Morawska, L., Afshari, A., Bae, G.N., Buonanno, G., Chao, C.Y., Hanninen, O., Hofmann, W., Isaxon, C., Jayaratne, E.R., Pasanen, P., Salthammer, T., Waring, M. and Wierzbicka, A. (2013). Indoor Aerosols: From Personal Exposure to Risk Assessment. *Indoor Air* 23: 462–487.

Oberdörster, G., Sharp, Z., Atudorei, V., Elder, A., Gelein, R., Kreyling, W. and Cox, C. (2004). Translocation of Inhaled Ultrafine Particles to the Brain. *Inhalation Toxicol.* 16: 437–445.

Oberdörster, G., Oberdörster, E. and Oberdörster, J. (2005). Nanotoxicology: An Emerging Discipline Evolving from Studies of Ultrafine Particles. *Environ. Health Perspect.* 113: 823–839.

Shin, W.G., Qi, C., Wang, J., Fissan, H. and Pui, D.Y.H. (2009). The Effect of Dielectric Constant of Materials on Unipolar Diffussion Charging on Nanoparticles. *J. Aerosol Sci.* 40: 463–468.

Shiue, A., Hu, S.C. and Tu, M.L. (2011). Particles Removal by Negative ionic Air Purifier in Cleanroom. *Aerosol Air Qual. Res.* 11: 179–186.

Song, Y., Li, X. and Du, X. (2009). Exposure to Nanoparticles is Related to Pleural Effusion, Pulmonary Fibrosis and Granuloma. *Eur. Respir. J.* 34: 559–567.

Sze-To, G.N., Wu, C.L., Chao, C.Y., Wan, M.P. and Chan, T.C. (2012). Exposure and Cancer Risk Toward Cooking-Generated Ultrafine and Coarse Particles in Hong Kong Homes. *HVAC&R Res.* 18: 204–216.

Wang, X., Chiu, Y., Qiu, H., Au, J. and Yu, I. (2009). The Roles of Smoking and Cooking Emissions in Lung Cancer Risk Among Chinese Women in Hong Kong. *Ann. Oncol.* 20: 746–751.

Waring, M.S., Siegel, J.A. and Corsi, R.L. (2008). Ultrafine Particle Removal and Generation by Portable Air Cleaners. *Atmos. Environ.* 42: 5003–5014.

Wu, C., Lee, G., Cheng, P., Yang, S. and Yu, K. (2006). Effect of Wall Surface Materials on Deposition of Particles with the Aid of Negative Air Ions. *J. Aerosol Sci.* 37: 616–630.

Yu, K.P. (2012). Enhancement of the Deposition of Ultrafine Secondary Organic Aerosols by the Negative Air Ion and the Effect of Relative Humidity. *J. Air Waste Manage. Assoc.* 62: 1296–1304.

Zhao, B., Zhang, Y., Li, X., Yang, X. and Huang, D. (2004). Comparison of Indoor Aerosol Particle Concentration and Deposition in Different Ventilated Rooms by Numerical Method. *Build. Environ.* 39: 1–8.

Zhao, B. and Wu, J. (2006). Modeling Particle Deposition onto Rough Walls in Ventilation Duct. *Atmos. Environ.* 40: 6918–6927.

Received for review, August 15, 2014
Revised, November 30, 2014
Accepted, January 14, 2015